Inverse Mpemba Effect Demonstrated on a Single Trapped Ion Qubit

Shahaf Aharony Shapira [ORCID],[*,†] Yotam Shapira,[*] Jovan Markov [ORCID], Gianluca Teza [ORCID], Nitzan Akerman,
Oren Raz, and Roee Ozeri

Department of Physics of Complex Systems, Weizmann Institute of Science, Rehovot 7610001, Israel

The Mpemba effect is a counterintuitive phenomena in which a hot system reaches a cold temperature faster than a colder system, under otherwise identical conditions. Here, we propose a quantum analog of the Mpemba effect, on the simplest quantum system, a qubit. Specifically, we show it exhibits an inverse effect, in which a cold qubit reaches a hot temperature faster than a hot qubit. Furthermore, in our system a cold qubit can heat up exponentially faster, manifesting the strong version of the effect. This occurs only for sufficiently coherent systems, making this effect quantum mechanical, i.e., due to interference effects. We experimentally demonstrate our findings on a single ^{88}Sr$^+$ trapped ion qubit. The existence of this anomalous relaxation effect in simple quantum systems reveals its fundamentality, and may have a role in designing and operating quantum information processing devices.

Physical systems undergoing relaxation can exhibit a wide range of rich and nontrivial phenomena. A prominent example is the Mpemba effect (ME) [1,2], in which an initially hot system cools down faster than a colder, otherwise identical, system. Some systems manifest a stronger version of this effect [3], in which the hotter system relaxes exponentially faster. The ME has been experimentally demonstrated in various classical systems, e.g., water [2], Clathrate hydrates [4], magnetic alloys [5], colloids diffusing in a potential [6], and a few others [7–9]. An inverse ME, in which an initially colder system heats up faster than a warmer system, has been predicted [10,11] and recently measured [12]. Much theoretical insight was gained on this effect in recent years, using various theoretical methods [13–23] and numerical results [24–27].

Theoretical quantum versions of the ME have been recently proposed in various models, e.g., Ising model [28], Anderson model [29], and a perturbative technique for Markovian open systems [30]. Quantum Mpemba-like theories, which are nonthermal, have also been suggested, including accelerated relaxation of dissipative open systems [31,32] and relaxation of entanglement asymmetry in spin systems [33–35]. The latter has been recently demonstrated using trapped-ions [36].

Here, we propose and experimentally demonstrate the existence of an inverse ME in the simplest quantum system —a single qubit. Our analysis shows that a strong inverse ME occurs for a sufficiently coherent qubit, making this effect quantum mechanical, i.e., due to interference.

We consider a coherently driven qubit that is coupled to a thermal Markovian bath, causing decoherence of the qubit and its eventual relaxation to a nonequilibrium steady state. Our only assumption on the qubit-bath coupling is that the qubit's decoherence rate is monotonically increasing with

the bath's temperature. This occurs, e.g., for a black-body photon-emitting bath, such that the emission rate increases with temperature at every given wavelength, in particular, at resonance with the qubit's transition energy.

We demonstrate the inverse ME experimentally by implementing it on the Zeeman qubit, defined on a single trapped ^{88}Sr$^+$ ion. Figure 1 shows our model and the corresponding implementation on the ion's energy levels, detailed further below.
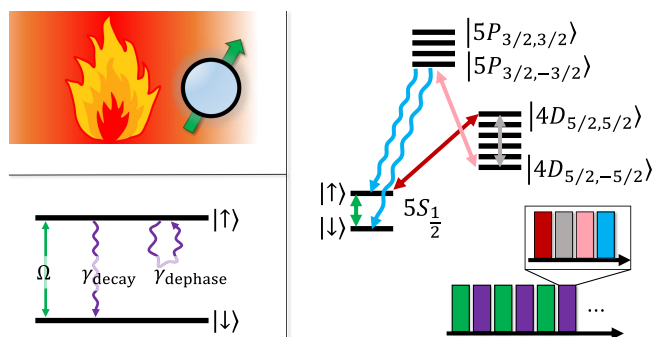
FIG. 1. Top left: the modeled quantum system exhibiting an inverse Mpemba effect. A thermal source of photons (fire) is coupled to coherently driven qubit (blue), causing it to relax to a steady state. Bottom left: the resulting coupling between the qubit's levels, $|\downarrow\rangle$ and $|\uparrow\rangle$, with a coherent drive (green) and decoherence terms causing decay (γ_{decay}) and dephasing (γ_{dephase}). Right: the qubit is mapped to the $5S_{1/2}$ levels of the Zeeman ground state manifold of a trapped ^{88}Sr$^+$ ion. Coherent (green) and incoherent (purple) dynamics are interlaced in order to generate the overall system evolution (pulse sequence). The incoherent dynamics are generated using states in the long-lived $4D_{5/2}$ and short-lived $5P_{3/2}$ manifolds with various transitions (red, gray, pink, and cyan), detailed below.

The qubit's dynamics is given by the Gorini-Kossakowski-Sudarshan-Lindblad (GKSL) equation, $\partial_t \rho = \mathcal{L}[\rho]$, with $\mathcal{L}$ a Lindblad superoperator, acting on $\rho \in \mathbb{C}^{2 \times 2}$, the density matrix representing a statistical ensemble of a single qubit. Specifically, the operation of the superoperator is given by ($\hbar = 1$),

$$\mathcal{L}[\rho] = -\frac{i\Omega}{2}[\sigma_x, \rho] + \gamma_{\text{decay}} L_{|\uparrow\rangle\langle\downarrow|}[\rho] + \gamma_{\text{dephase}} L_{|\uparrow\rangle\langle\uparrow|}[\rho], \quad (1)$$

with Ω the rate of the coherent driving of the qubit, set by the x-Pauli matrix σ_x. Open Markovian dynamics are generated by $L_A[\rho] \equiv A\rho A^\dagger - \frac{1}{2}\{A^\dagger A, \rho\}$. We consider decoherence due to decay (dephasing), generated by $|\downarrow\rangle\langle\uparrow|$ ($|\uparrow\rangle\langle\uparrow|$), with rates,

$$\gamma_{\text{decay}} = \alpha\gamma(T), \qquad \gamma_{\text{dephase}} = (1-\alpha)\gamma(T), \quad (2)$$

where $\alpha \in [0,1]$ is the relative occurrence of decay with respect to the decoherence rate and $\gamma(T)$ is the overall temperature-dependent decoherence rate due to coupling to the bath [37]. Throughout this work, the qubit's temperature is defined once it reaches a steady state with the bath. We note that $\gamma(T)$ is assumed to be monotonically increasing with T, e.g., via Planck's law, such that we can characterize the bath and the steady state temperature by T or γ interchangeably.

The dynamics is conveniently analyzed using the Bloch vector, $\vec{r} = (x, y, z)$, with $\rho = (1/2)(1 + \vec{r} \cdot \vec{\sigma})$ [see derivation in Supplemental Material (SM) [38]]. Since the system is driven, its fixed points correspond to non-equilibrium steady states that do not obey detailed balance, e.g., the qubit continuously scatters photons and its long-time limit is not $\propto e^{-\beta H}$. The collection of steady states, $\vec{r}^{\text{ss}}(\gamma)$, form a right half of an ellipse in the y–z plane, with its center at $(0, 0, -1/2)$ and semiaxes $(r_y, r_z) = (\sqrt{\alpha}/2, 1/2)$, shown in Fig. 2 (left). Each point on this curve, known as the steady state locus, corresponds to a steady state at a given $\gamma' \equiv \gamma/\Omega$, with $\gamma' \to 0(\infty)$ corresponding to the center (south pole) of the Bloch sphere.

Consider the relaxation path of an initial condition given by the steady state solution of a cold temperature $\vec{r}^{\text{ss}}(\gamma_i)$ when coupled to a hot bath characterized by γ_f. The solution of Eq. (1) is then given by

$$\vec{r}(t; \gamma_i, \gamma_f) = \vec{r}^{\text{ss}}(\gamma_f) + \sum_{n \in \{+,-,x\}} a_n(\gamma_i, \gamma_f)\vec{v}_n(\gamma_f)e^{\lambda_n(\gamma_f)t}, \quad (3)$$

where $\vec{v}_n(\gamma_f)$ are the relaxation modes of the system, $\lambda_n(\gamma_f)$ their rates, and $a_n(\gamma_i, \gamma_f)$ the corresponding coefficients, determined by the overlap between the initial state and $\vec{v}_n(\gamma_f)$.

We note that the x coordinate has a stable fixed point at $x^* = 0$, making the x direction trivially vanish throughout the system's evolution.
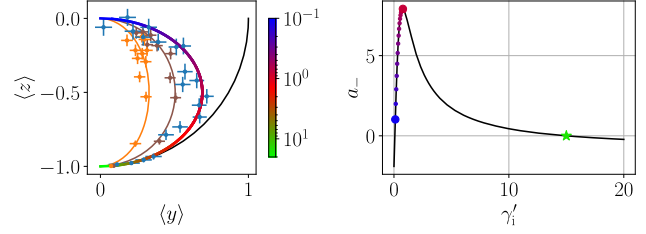
FIG. 2. Left: steady state locus. We measure the qubit's steady-state position (points) on the y-z plane of the Bloch sphere (black line) at different temperatures and compute the corresponding α's (see the main text). Our datasets (points) are fitted yielding $\alpha = 0.21 \pm 0.03$ (orange), $\alpha = 0.51 \pm 0.04$ (brown), and $\alpha = 0.94 \pm 0.07$ (blue), used hereafter. The steady state locus corresponding to the latter is presented in color, showing values of γ' (log scale). Error bars correspond to $\pm 2\sigma$ confidence intervals due to the quantum shot noise of 300 experimental repetitions. Right: coefficient of the slow-decaying eigenstate a_- as a function of γ'_i, for $\gamma'_f = 15$ (green star). The coefficient shows a nonmonotonic behavior, implying the existence of a ME. Furthermore, the curve is shown to vanish at $\gamma'_i = 0.07$, proving the existence of a strong ME. The highlighted points correspond to the γ'_i's in Fig. 3.

The decay rates in the y-z plane are given by the real part $\text{Re}[\lambda_\pm]$, with

$$\lambda_\pm = -\gamma_f\left(\alpha + 1/2 \pm \sqrt{(\alpha - 1/2)^2 - 1/\gamma_f'^2}\right). \quad (4)$$

The ME can exist only when $\text{Re}[\lambda_\pm]$ are distinct, allowing for slow and fast relaxation modes. This occurs for final temperatures $\gamma'_f > \gamma'_b$, with the bifurcation point $\gamma'_b \equiv |\alpha - 1/2|^{-1}$.

The relaxation at long times is determined by the slowest relaxation mode λ_- and its coefficient a_-, which clearly vanishes for $\gamma_i = \gamma_f$. Fixing γ'_f, one might expect a_- to be monotonic in the range $0 \leq \gamma'_i \leq \gamma'_f$. However, for an inverse ME to take place, a cold system must reach the steady state faster than a hotter one, i.e., $|a_-|$ is smaller for a cold system, compared to a hotter system. It is therefore the nonmonotonic behavior of a_- as a function of γ_i which enables the existence of the ME [3]. Indeed, the coefficient $a_-(\gamma_i, \gamma_f)$ displays such a behavior, implying the existence of an inverse ME. An example with $\gamma'_f = 15$ is plotted in Fig. 2 (right).

A strong ME occurs in the special case in which a_- vanishes at an initial temperature, $\gamma_{i,\text{SME}} \neq \gamma_f$. In that case, the relaxation time is determined by the fast rate λ_+, and as a result, it is exponentially faster [3]. In other words, defining the distance to steady state, $d_{\text{ss}}^{\gamma_i}(t) \equiv |\vec{r}(t; \gamma_i, \gamma_f) - \vec{r}^{\text{ss}}(\gamma_f)|$, then $d_{\text{ss}}^{\gamma_i \neq \gamma_{i,\text{SME}}}(t)/d_{\text{ss}}^{\gamma_{i,\text{SME}}}(t)$ is asymptotically exponentially increasing in time.

Here, a_- vanishes at $\gamma'_{i,\text{SME}} = \gamma'_f\left((\alpha - 1/2) - \sqrt{(\alpha - 1/2)^2 - \gamma'^{-2}_f}\right)$. For example, for $\gamma'_f = 15$, a_- vanishes at $\gamma'_{i,\text{SME}} \approx 0.07$ as seen in Fig. 2 (right). The strong ME in this system is experimentally optimal to achieve the

most pronounced signal. Indeed, in our experimental demonstrations we make use of values $\gamma_i \approx \gamma_{i,SME}$. We mathematically prove the strong ME can only appear in a heating process, i.e., as an inverse ME (see SM [38]).

Since $\gamma'_{i,SME} > 0$, the required α for a strong ME is bounded by $\alpha > 1/2 + 1/\gamma'_f \geq 1/2$. When α satisfies this condition, there exists a strong ME for every final temperature above the bifurcation point, at $\gamma'_{i,SME}$. Thus, an exponentially faster relaxation occurs only in a sufficiently coherent system, i.e., with a low excess dephasing on top of that induced by the decay channel. Specifically, a classical bit, with no coherence between its two states, cannot exhibit this strong effect.

This model describes, for example, a single trapped $^{88}Sr^+$ ion qubit in a small-scale quantum computer [39]. Specifically we encode the $|\downarrow\rangle$ ($|\uparrow\rangle$) qubit state on the $5S_{1/2,-1/2}$ ($5S_{1/2,1/2}$) state in the Zeeman ground state manifold, shown in Fig. 1 (right). The two states are coherently coupled with a magnetic field (green), oscillating at the Zeeman splitting frequency in the $5S_{1/2}$ manifold, generating the qubit's Hamiltonian, $H = \Omega\sigma_x/2$, with Ω the field's Rabi frequency.

As shown in Fig. 1, we combine the coherent and open dynamics in discrete steps, by interlacing small durations of coherent (green pulse) and open Markovian evolution (purple pulse), i.e., by Trotterization. Markovian open dynamics are generated by coupling the qubit levels via fast decaying states [40]. Control over γ and α is gained by making use of the sequential cascade of pulses and transitions.

Specifically, we use a narrow linewidth laser at 674 nm [41] (red) in order to selectively couple the $|\uparrow\rangle$ state to the $|4D_{5/2,5/2}\rangle$ state in the $4D_{5/2}$ metastable manifold. An additional laser at 1033 nm (pink) couples the $4D_{5/2}$ manifold to the short-lived $5P_{3/2}$. Because of selection rules, only the $|5P_{3/2,3/2}\rangle$ state is populated, which quickly decays back to the $|\uparrow\rangle$ state (blue), resulting in full dephasing, i.e., $\alpha = 0$. By using an additional π pulse in the $4D_{5/2}$ manifold (gray), between the 674 nm and the 1033 nm pulses, we map the $|4D_{5/2,5/2}\rangle$ state to the $|4D_{5/2,-5/2}\rangle$, which will ultimately decay to the $|\downarrow\rangle$ state, yielding $\alpha \approx 1$. The value of γ is determined by the 674 nm pulse amplitude and length, as these control the relative population that is excited outside of the $5S_{1/2}$ qubit manifold in each pulse cycle.

We demonstrate this control experimentally by initializing the system to the $|\uparrow\rangle$ state and letting it relax to a steady state under $n = 100$ repetitions of interlaced dynamics, analogous to a decay time of $7\gamma_f^{-1}$. After this evolution we perform state tomography to determine the location of the steady state on the Bloch sphere. Figure 2 (left) shows the measured steady states for various values of γ', forming the elliptically shaped steady state locus (blue points), with a fitted value of $\alpha = 0.94 \pm 0.07$ (gradient line).
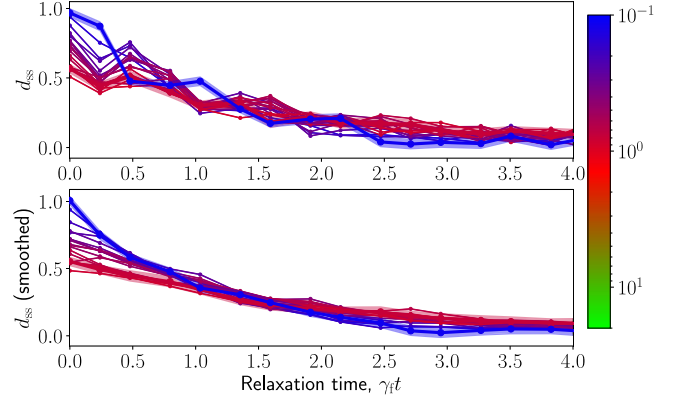
FIG. 3. The inverse ME is demonstrated by relaxing qubits to a steady state at various initial temperatures, γ'_i (color), and tracking their relaxation as a function of time (horizontal) to a final steady state at a fixed temperature, $\gamma'_f = 15 > \gamma'_i$ and $\alpha = 0.94$. We consider the qubit's Euclidean distance to the final steady state, $d_{ss}(t)$ (vertical). We highlight an initially cold (thick blue) and hot (thick red) systems, d_{ss}^C and d_{ss}^H, analyzed further below. Error regions correspond to $\pm 2\sigma$ confidence intervals due to the quantum shot noise of 400 experimental repetitions. Top: d_{ss} exhibits oscillations, not captured by the model above, which occur due to the relatively large time steps used in the evolution. Bottom: postprocessing the same data by polynomial smoothing reproduces the inverse ME. Specifically, $d_{ss}^C > d_{ss}^H$ at $t = 0$, however, their values cross at $t \approx 2\gamma_f^{-1}$, after which $d_{ss}^C < d_{ss}^H$.

Intermediate values of α can be formed by replacing the π pulse in the $4D_{5/2}$ manifold (gray) with, e.g., a $\pi/2$ pulse or a $\pi/5$ pulse, yielding a thinner steady state loci, fitted as $\alpha = 0.51 \pm 0.04$ and $\alpha = 0.21 \pm 0.03$ (brown and orange), respectively.

A canonical experimental protocol for measuring the ME comprises letting the system relax to the steady state $\vec{r}^{ss}(\gamma'_i)$, then quenching it to a final temperature γ'_f while performing tomography of the relaxation dynamics to $\vec{r}^{ss}(\gamma'_f)$. The measurements are then used to obtain the Euclidean distance on the Bloch sphere from the final steady state, $d_{ss}(t)$. This protocol raises a technical challenge, namely, the relaxation time to an initial cold system, with $\gamma'_i \ll 1$, requires a long evolution duration, which may surpass the system's natural coherence time, leading to an effectively reduced and uncontrolled value of α.

We mitigate this challenge by measuring the ME using two complementary techniques: performing the experimental protocol with large Trotter steps, thus reducing the total duration of an experiment, or by effectively preparing the qubit in the initial state, $\vec{r}^{ss}(\gamma'_i)$, thus circumventing the long initial relaxation time.

The results obtained by the former technique, large Trotter steps, are shown in Fig. 3. Specifically, we evolve the system to $t = 4\gamma_f^{-1}$ in 14 Trotter steps (horizontal) and present $d_{ss}(t)$ (vertical) for various γ'_i's (color). These steps form a less accurate approximation of the continuous model. Indeed,
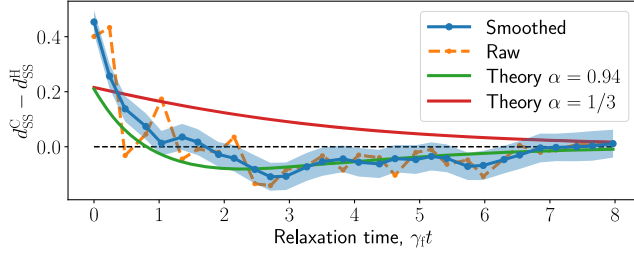
FIG. 4. Comparison between raw and smoothed data (orange and blue, respectively) and corresponding analytical predictions of the difference between distances from final state, $d_{ss}^C - d_{ss}^H$. The inverse ME seen as a negative value of the smoothed data, beyond the error bars, agrees with our prediction for $\alpha = 0.94$ (green). The coherence requirement is exemplified by presenting an alternative prediction, with $\alpha = 1/3$ (red), below the minimal value for a strong ME, which indeed shows no effect.

Fig. 3 (top) exhibits oscillations which are common to nonadiabatic digitized evolution. We compensate for the oscillations by employing simple polynomial smoothing of the data, shown in Fig. 3 (bottom).

We highlight an initially cold system, $\gamma_i'^C = 0.116$ (blue) and an initially hot system, $\gamma_i'^H = 0.776$ (red). These demonstrate an inverse ME, as the curves of the cold and hot systems cross, with the cold system reaching the steady state before the hot system.

Figure 4 presents the distance between these two systems during relaxation, $d_{ss}^C(t) - d_{ss}^H(t)$, for the raw data (orange) and smoothed data (blue). Indeed, $d_{ss}^C(0) - d_{ss}^H(0) > 0$, indicating the cold system is initially at a larger distance from steady state. However, during the relaxation we observe a crossing time t_{cross} after which $d_{ss}^C(t) - d_{ss}^H(t) < 0$, beyond $\pm 2\sigma$ error bars due to quantum shot noise. The theoretical prediction for this distance at $\alpha = 0.94$ is shown (green), with a well correspondence to the data. Furthermore we show the theoretical prediction for the case, $\alpha = 1/3$, outside of the strong-ME regime, in which no crossing is observed (red).

Next, we directly prepare the qubit at an initial steady state. We write the initial steady state density matrix, ρ_i^{ss}, as a linear combination of two pure states. Here, the steady states are all of the form, $\rho_i^{ss} = [(1-p)/2]|+\theta\rangle\langle+\theta| + [(1+p)/2]|-\theta\rangle\langle-\theta|$, with θ and p representing the direction and distance of the steady state from the Bloch sphere origin and $|\pm\theta\rangle \equiv \exp\{-(i/2)[\theta \pm (\pi/2)]\sigma_x\}|\uparrow\rangle$ [38]. Then, the evolution of ρ_i^{ss} is equivalent to the same linear combination of evolved pure states. Observables stemming from the evolution of ρ_i^{ss}, are recovered by measuring the same observables on the evolution of $|\pm\theta\rangle$, and using a weighted linear combination of the results, with weights $(1\mp p)/2$.

Figure 5 shows the dynamics of system initialized at steady states with respect to various γ_i''s, and tracks their evolution as a function of time (horizontal) toward a fixed $\gamma_f' = 100 > \gamma_i'$. Similarly to Fig. 3, we show the distance to
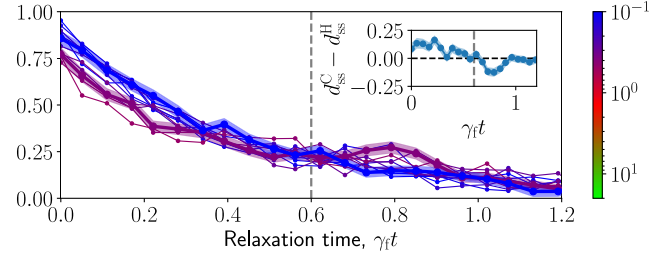
FIG. 5. The inverse ME realized with initial state preparation. The qubit's distance to the final steady state $d_{ss}(t)$ is shown for qubits initialized at different temperatures (color) and quenched to $\gamma_f' = 100$ and $\alpha = 0.94$. We highlight d_{ss}^C (thick dark blue) and d_{ss}^H (thick light blue), initially cold and hot systems, respectively, and present their $\pm 2\sigma$ confidence intervals (shaded regions). As shown, the hot qubit starts closer to the final steady state. However, at $t_{cross} \approx 0.6\gamma_f^{-1}$ (vertical gray) the cold system surpasses the hot system and relaxes first, manifesting the inverse Mpemba effect. Error bars (shaded regions) correspond to $\pm 2\sigma$ confidence intervals due to the quantum shot noise of 400 experimental repetitions. Inset: $d_{ss}^C(t) - d_{ss}^H(t)$ highlighting the crossing of the two systems, beyond the confidence intervals.

the final steady state d_{ss} and highlight an initially cold, $\gamma_i'^C \approx 0$ (blue) and hot, $\gamma_i'^H = 0.390$ (purple) systems. As above, $d_{ss}^C(0) > d_{ss}^H(0)$, indicating the cold system is initially at a larger distance from steady state, yet during the relaxation we observe a crossing time t_{cross} after which $d_{ss}^C(t) < d_{ss}^W(t)$, beyond error bars. This is also reflected in the inset which shows $d_{ss}^C - d_{ss}^H$ (vertical) initially positive and at later times negative, beyond the error bars.

In conclusion, we have proposed and experimentally demonstrated the inverse ME on as single qubit. Furthermore, we have proven that a strong, i.e., exponentially faster relaxation, ME exists only for a sufficiently coherent qubit. As our findings pertain the simplest quantum system, one expects to find the ME in larger quantum systems, such as quantum computers, in which maintaining a low temperature for long times is crucial.

---

[*]These authors contributed equally to this letter.
[†]shahaf.aharony@weizmann.ac.il

[1] E. B. Mpemba and D. G. Osborne, Cool?, Phys. Educ. **4**, 172 (1969).

[2] M. Jeng, The Mpemba effect: When can hot water freeze faster than cold?, Am. J. Phys. 74, 514 (2006).

[3] I. Klich, O. Raz, O. Hirschberg, and M. Vucelja, Mpemba index and anomalous relaxation, Phys. Rev. X 9, 021060 (2019).

[4] Y.-H. Ahn, H. Kang, D.-Y. Koh, and H. Lee, Experimental verifications of Mpemba-like behaviors of clathrate hydrates, Korean J. Chem. Eng. 33, 1903 (2016).

[5] P. Chaddah, S. Dash, K. Kumar, and A. Banerjee, Overtaking while approaching equilibrium, arXiv:1011.3598.

[6] A. Kumar and J. Bechhoefer, Exponentially faster cooling in a colloidal system, Nature (London) 584, 64 (2020).

[7] C. Hu, J. Li, S. Huang, H. Li, C. Luo, J. Chen, S. Jiang, and L. An, Conformation directed Mpemba effect on polylactide crystallization, Cryst. Growth Des. 18, 5757 (2018).

[8] J. Liu, J. Li, B. Liu, I. W. Hamley, and S. Jiang, Mpemba effect in crystallization of polybutene-1, Soft Matter 19, 3337 (2023).

[9] M. Chorazewski, M. Wasiak, A. V. Sychev, V. I. Korotkovskii, and E. B. Postnikov, The curious case of 1-ethylpyridinium triflate: Ionic liquid exhibiting the Mpemba effect, J. Solution Chem. 53, 80 (2024).

[10] Z. Lu and O. Raz, Nonequilibrium thermodynamics of the Markovian Mpemba effect and its inverse, Proc. Natl. Acad. Sci. U.S.A. 114, 5083 (2017).

[11] A. Lasanta, F. Vega Reyes, A. Prados, and A. Santos, When the hotter cools more quickly: Mpemba effect in granular fluids, Phys. Rev. Lett. 119, 148001 (2017).

[12] A. Kumar, R. Chétrite, and J. Bechhoefer, Anomalous heating in a colloidal system, Proc. Natl. Acad. Sci. U.S.A. 119, e2118484119 (2022).

[13] M. R. Walker and M. Vucelja, Anomalous thermal relaxation of Langevin particles in a piecewise-constant potential, J. Stat. Mech. (2021) 113105.

[14] R. Holtzman and O. Raz, Landau theory for the Mpemba effect through phase transitions, Commun. Phys. 5, 280 (2022).

[15] J. Degünther and U. Seifert, Anomalous relaxation from a non-equilibrium steady state: An isothermal analog of the Mpemba effect, Europhys. Lett. 139, 41002 (2022).

[16] D. M. Busiello, D. Gupta, and A. Maritan, Inducing and optimizing Markovian Mpemba effect with stochastic reset, New J. Phys. 23, 103012 (2021).

[17] G. Teza, R. Yaacoby, and O. Raz, Eigenvalue crossing as a phase transition in relaxation dynamics, Phys. Rev. Lett. 130, 207103 (2023).

[18] F. J. Schwarzendahl and H. Löwen, Anomalous cooling and overcooling of active colloids, Phys. Rev. Lett. 129, 138002 (2022).

[19] S. Zhang and J.-X. Hou, Theoretical model for the Mpemba effect through the canonical first-order phase transition, Phys. Rev. E 106, 034131 (2022).

[20] G. Teza, R. Yaacoby, and O. Raz, Relaxation shortcuts through boundary coupling, Phys. Rev. Lett. 131, 017101 (2023).

[21] A. Biswas, V. V. Prasad, O. Raz, and R. Rajesh, Mpemba effect in driven granular Maxwell gases, Phys. Rev. E 102, 012906 (2020).

[22] A. Santos and A. Prados, Mpemba effect in molecular gases under nonlinear drag, Phys. Fluids 32, 072010 (2020).

[23] R. Chétrite, A. Kumar, and J. Bechhoefer, The metastable Mpemba effect corresponds to a non-monotonic temperature dependence of extractable work, Front. Phys. 9, 141 (2021).

[24] M. Baity-Jesi, E. Calore, A. Cruz, L. A. Fernandez, J. M. Gil-Narvión, A. Gordillo-Guerrero, D. Iñiguez, A. Lasanta, A. Maiorano, E. Marinari et al., The Mpemba effect in spin glasses is a persistent memory effect, Proc. Natl. Acad. Sci. U.S.A. 116, 15350 (2019).

[25] A. Gal and O. Raz, Precooling strategy allows exponentially faster heating, Phys. Rev. Lett. 124, 060602 (2020).

[26] A. Gijón, A. Lasanta, and E. R. Hernández, Paths towards equilibrium in molecular systems: The case of water, Phys. Rev. E 100, 032103 (2019).

[27] N. Vadakkayil and S. K. Das, Should a hotter paramagnet transform quicker to a ferromagnet? Monte Carlo simulation results for Ising model, Phys. Chem. Chem. Phys. 23, 11186 (2021).

[28] A. Nava and M. Fabrizio, Lindblad dissipative dynamics in the presence of phase coexistence, Phys. Rev. B 100, 125102 (2019).

[29] A. K. Chatterjee, S. Takada, and H. Hayakawa, Quantum Mpemba effect in a quantum dot with reservoirs, Phys. Rev. Lett. 131, 080402 (2023).

[30] F. Ivander, N. Anto-Sztrikacs, and D. Segal, Hyperacceleration of quantum thermalization dynamics by bypassing long-lived coherences: An analytical treatment, Phys. Rev. E 108, 014130 (2023).

[31] F. Carollo, A. Lasanta, and I. Lesanovsky, Exponentially accelerated approach to stationarity in Markovian open quantum systems through the Mpemba effect, Phys. Rev. Lett. 127, 060401 (2021).

[32] S. Kochsiek, F. Carollo, and I. Lesanovsky, Accelerating the approach of dissipative quantum spin systems towards stationarity through global spin rotations, Phys. Rev. A 106, 012207 (2022).

[33] F. Ares, S. Murciano, and P. Calabrese, Entanglement asymmetry as a probe of symmetry breaking, Nat. Commun. 14, 2036 (2023).

[34] S. Murciano, F. Ares, I. Klich, and P. Calabrese, Entanglement asymmetry and quantum Mpemba effect in the XY spin chain, J. Stat. Mech. 013103 (2024).

[35] C. Rylands, K. Klobas, F. Ares, P. Calabrese, S. Murciano, and B. Bertini, Microscopic origin of the quantum Mpemba effect in integrable systems, arXiv:2310.04419.

[36] L. K. Joshi, J. Franke, A. Rath, F. Ares, S. Murciano, F. Kranzl, R. Blatt, P. Zoller, B. Vermersch, P. Calabrese, C. F. Roos, and M. K. Joshi, preceding Letter, Observing the quantum Mpemba effect in quantum simulations, Phys. Rev. Lett. 133, 010402 (2024).

[37] G. McCauley, B. Cruikshank, D. I. Bondar, and K. Jacobs, Accurate Lindblad-form master equation for weakly damped quantum systems across all regimes, npj Quantum Inf. 6, 74 (2020).

[38] See Supplemental Material at http://link.aps.org/supplemental/10.1103/PhysRevLett.133.010403, for additional derivation and technical information.

[39] T. Manovitz, Y. Shapira, L. Gazit, N. Akerman, and R. Ozeri, Trapped-ion quantum computer with robust entangling gates and quantum coherent feedback, PRX Quantum 3, 010347 (2022).

[40] E. Ben Av, Y. Shapira, N. Akerman, and R. Ozeri, Direct reconstruction of the quantum-master-equation dynamics of a trapped-ion qubit, Phys. Rev. A **101,** 062305 (2020).

[41] L. Peleg, N. Akerman, T. Manovitz, M. Alon, and R. Ozeri, Phase stability transfer across the optical domain using a commercial optical frequency comb system, arXiv:1905.05065.